V European Conference on Computational Fluid Dynamics
ECCOMAS CFD 2010
J. C. F. Pereira and A. Sequeira (Eds)
Lisbon, Portugal,14-17 June 2010

DEVELOPMENT OF A GENERIC SURFACE MAPPING ALGORITHM FOR FLUID-STRUCTURE-INTERACTION SIMULATIONS IN TURBOMACHINERY

Christian Voigt*, Christian Frey* and Hans-Peter Kersken†

*Institute of Propulsion Technology, German Aerospace Center (DLR)
†Simulation and Software Technology, German Aerospace Center (DLR)
Linder Hoehe, D-51147 Cologne, Germany
e-mail: {Christian.Voigt, Christian.Frey, Hans-Peter.Kersken}@dlr.de

Key words: TURBOMACHINERY, AEROELASTICITY, FLUID-STRUCTURE-INTERACTION

Abstract. *The practice of three dimensional time accurate computational fluid dynamics (CFD) methods and the use of computational structural mechanics solver (CSM) are essential for the turbomachinery design process. New technologies like the blisk design for aeroengines or the increased requirements on flexible loading of stationary gas or steam turbines for power generation makes a tight integration and coupling of both CFD and CSM tools indispensable. Especially the effects of fluid-structure-interaction (FSI) are an important field for investigations even in early stages of the modern design and optimization process.*

The DLR in-house CFD code TRACE[1] *is a time accurate Reynolds-averaged Navier-Stokes-solver including a time linearized module developed for the efficient investigation of FSI phenomena. The linear solver allows to reduce response times for flutter calculations by up to two orders of magnitude compared to nonlinear time accurate calculations[2]. Combined with the CSM solver CalculiX[3] a process chain for aeroelastic design optimization for turbomachinery is established. An essential ingredient of this process is the mapping of surface displacements computed by the CSM solver onto the mesh of the CFD solver. A mapping algorithm has been implemented which does not rely on topology information, e.g. the position of the leading and trailing edge of a blade, but uses geometric data, i.e. vertex coordinates and surface elements,only.*

The focus of this article will be on the algorithms for a topology independent mapping including the approximation of the structural model and the handling of complex mode shapes. The application of this algorithm to a turbine vane and high pressure turbine blade cluster is presented. The process for flutter investigations is shown for a high pressure ratio single stage fan.

1 INTRODUCTION

The motivation for the development of an aeroelastic pre-processor PREP was to implement an algorithm of industrial strength to provide the results of a CSM solver to the CFD solver TRACE for aeroelastic applications.

PREP transfers (maps) the surface displacements computed by a CSM solver on a finite element grid to the respective boundaries of the CFD mesh. Special attention was paid to an automatic process with the least possible user intervention needed in order to enable automatic, script controlled workflow. Therefore strategies were employed to ensure the mapping for arbitrary topologies. In the following the application to aeroelastic calculations is presented where the mapped surface displacements are used to deform the CFD mesh to investigate blades with respect to their flutter behavior.

The algorithm basically consists of three steps. The first is the automatic alignment of the CSM and CFD geometries. The second is the mapping of the surface displacements from the CSM data to the CFD boundaries. The third is the calculation of the mesh deformation.

The following three sections describe this algorithm in detail followed by a section showing results of the application to the 11th standard configuration[4,5], to a welded low pressure turbine blade cluster and a high pressure single stage fan.

2 ALIGNMENT OF THE GEOMETRIES

To align the CSM and CFD geometries is the first step in the presented algorithm. For an industrial workflow it is mandatory that the alignment is performed fully automatic without user knowledge of the given geometries. The only input to PREP is the specification of the CFD mesh surface regions onto which the CSM surface displacements should be mapped. No further user interaction is required. Nevertheless there are some possibilities to influence the matching process, for example to mirror the CSM geometry about planes spanned by two arbitrary coordinate axes, to perform additional shifts and rotations or to control the automatic alignment to test the best strategy for the current process.

In essence the alignment is a coordinate transformation performed on the CSM data to map it into the domain of the CFD geometry's system. Each system is spanned by the principle axes of the specified surface and the center of area as its origin. Let A_i and $\mathbf{r}_i$ be the area and the face center of the i-th element, respectively. Then the center of area $\mathbf{x}_0$ can easily be obtained by calculating the area weighted average of the N element face centers:

$$\mathbf{x}_0 = \frac{\sum_{i=1}^{\mathrm{N}} \mathrm{A}_i \, \mathbf{r}_i}{\sum_{i=1}^{\mathrm{N}} \mathrm{A}_i} \, . \tag{1}$$

The system's axes are the eigenvectors of a system similar to the moment of inertia tensor $\mathbf{I}$:

$$\mathbf{I} = \sum_{i=1}^{\mathrm{N}} \mathrm{A}_i (\|\mathbf{r}_i\|^2 \, \mathbf{Id} - \mathbf{r} \otimes \mathbf{r}) \; . \tag{2}$$

The simplification to just sum up the face areas and neglect the moments of inertia of every single face is sufficient for even coarse CSM grids and much finer CFD meshes. This approximation does not result in significant misalignment of the geometries.

The moment of inertia tensor is positive semi-definite and symmetric therefore the cyclic Jacobi method[6] to obtain the eigenvalues and eigenvectors is used. These eigenvectors are combined to the principal axes systems for CSM and CFD geometry. The order of the eigenvectors in the principal axes system of the CSM grid are sorted in the way that the order of the corresponding eigenvalues matches the ones of the CFD system, i.e. the euclidean norm for the difference of the vectors of eigenvalues is minimized. This way it can be assured that the CSM's and the CFD's axes system have the same orientation. If the systems show a different orientation, either right-hand or left-hand rule, the principal axes system of the CSM geometry is reorientated by axis inversion. To define the minimum rotation, caused by the subsequent transformation, different axis inversions will be applied until the Frobenius norm of the transformation matrix is minimized. The transformation matrix is the product of the principal axes systems $\mathbf{I}_0$ of the CSM and CFD geometry:

$$\mathbf{T} = \mathbf{I}_{0,\mathrm{CFD}} \, \mathbf{I}_{0,\mathrm{CSM}} \; . \tag{3}$$

The transformation matrix is applied from the left to the CSM grid and displacement vectors. For the coordinates this has to be done w.r.t. to the CSM geometry's moment of inertia reference frame:

$$\mathbf{x}_{\mathrm{CSM}}^{\mathrm{CFD}} = \mathbf{T} \, (\mathbf{x}_{\mathrm{CSM}} - \mathbf{x}_0) \; . \tag{4}$$

In which $\mathbf{x}_{\mathrm{CSM}}^{\mathrm{CFD}}$ are the CSM coordinates in the CFD's frame of reference.

The described approach fails for mirror-inverted geometries or significantly different CSM and CFD geometries. In this case user invention is required to supply additional information to the mapping algorithm as mentioned in beginning of this section.

3 MAPPING OF THE DATA

With the two geometries congruent the mapping itself is rather easy. In application the computation time of the mapping is negligible compared to the time consumption of the subsequent mesh deformation described below. Therefore a simple nearest neighbor search finding the CSM face nearest to a CFD mesh corner node is a valid and straight forward method. The CSM surface element with its face center nearest to the examined CFD mesh node is selected.

If the face diameters are large compared to the thickness of the blade, it happens that the nearest found element resides on the opposite side of the blade. To prevent this false pairing surface normals are taken into account. In the nearest neighbor search only CSM mesh elements are considered for which the face normal points into the same have space as the normal direction defined for the CFD mesh node examined. This normal direction is computed as the average of the normals of its adjacent faces.

Once the element nearest to the examined corner node is found an inverse distance weighting interpolation is performed. The sampling points are the corner nodes of the selected CSM surface elements. The limit of this approach is again a very coarse CSM grid in combination with a fine CFD mesh. In this cases a bilinear interpolation has to be performed.

4 DEFORMATION OF THE MESH

Once the surface displacement vectors are mapped onto the specified wall boundaries of the CFD mesh, a grid deformation is computed using an elliptic mesh deformation algorithm. The algorithm is based on the linear elasticity theory[7] for an elastic solid body subject to surface tractions prescribed by the surface displacement vectors. For the application to grid deformation the Poisson ratio is set to zero and the Young's modulus E is chosen to be proportional to the inverse cell volume. This inhibits deformation of small cells which are, however, displaced en bloc when adjacent cells change their form. The deformation vector $\tilde{\mathbf{x}}$ for each grid point is computed as the solution of the Poisson equation system

$$\nabla \cdot (E(\mathbf{x})\, \nabla \tilde{\mathbf{x}}) = f(x) \tag{5}$$

for the real and imaginary parts of the three cartesian components of $\tilde{\mathbf{x}}$. In absence of body forces f is zero. An iterative method is used to solve this Poisson equation system for the real and imaginary parts of the three cartesian components of $\tilde{\mathbf{x}}$. In order to reduce the CFD problem to one single passage, phase lag conditions are prescribed at periodic boundaries for the complex mesh deformations, i.e.

$$\tilde{\mathbf{x}}(\theta + \delta\theta) = e^{i\sigma}\, M_{\delta\theta}\, \tilde{\mathbf{x}}(\theta), \tag{6}$$

where $\delta\theta$ and σ denote the pitch and the interblade phase angle, respectively. Here, $M_{\delta\theta}$ is the rotation matrix for the rotation about the x-axis by $\delta\theta$.

The surface displacement is usually prescribed by inhomogeneous Dirichlet conditions for the three complex components. However, to avoid strong shearing of the tip clearance cells, we replace the Dirichlet condition by a slip wall condition. It prescribes the normal displacement but allows grid points to move tangentially to solid walls. Figure 1 shows the tip clearance region with the blade in the undeformed state and at the maximal deflections. Due to the slip wall condition no shearing of the near wall cells can be

observed. Notice that the correct computation of the shear stresses at solid walls, and thus the viscous fluxes of the flow solver, must not be based on the grid velocity as computed from the grid deformation vectors but on the actual wall movement defined by the surface displacements.

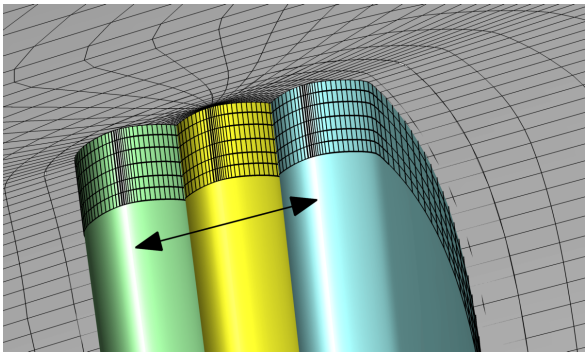

Figure 1: Original (yellow) and deformed tip clearence cells for maximal deflection (blue and green).

5 APPLICATIONS

5.1 STANDARD CONFIGURATION 11

The 11th standard configuration[4,5] describes a turbine vane in an annular nonrotating cascade. The test case shown here, the mapping of the third complex eigenmode and the subsequent mesh deformation, is a good example to explain the obstacles sometimes encountered in an industrial workflow.

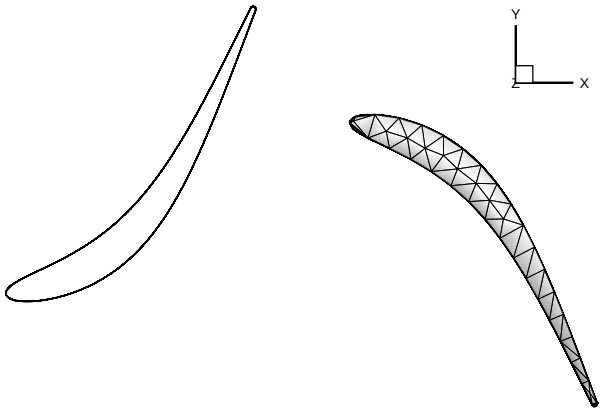

Figure 2: Orientation of the CSM geometry (right) and the CFD surface mesh (left) before the alignment.

The coarse unstructured CSM grid is applied to a mirrored geometry, see figure 2, that has a tip clearence while the CFD mesh has not. The difficulty is, that the described alignment algorithm matches the geometries without recognizing the different radial blade

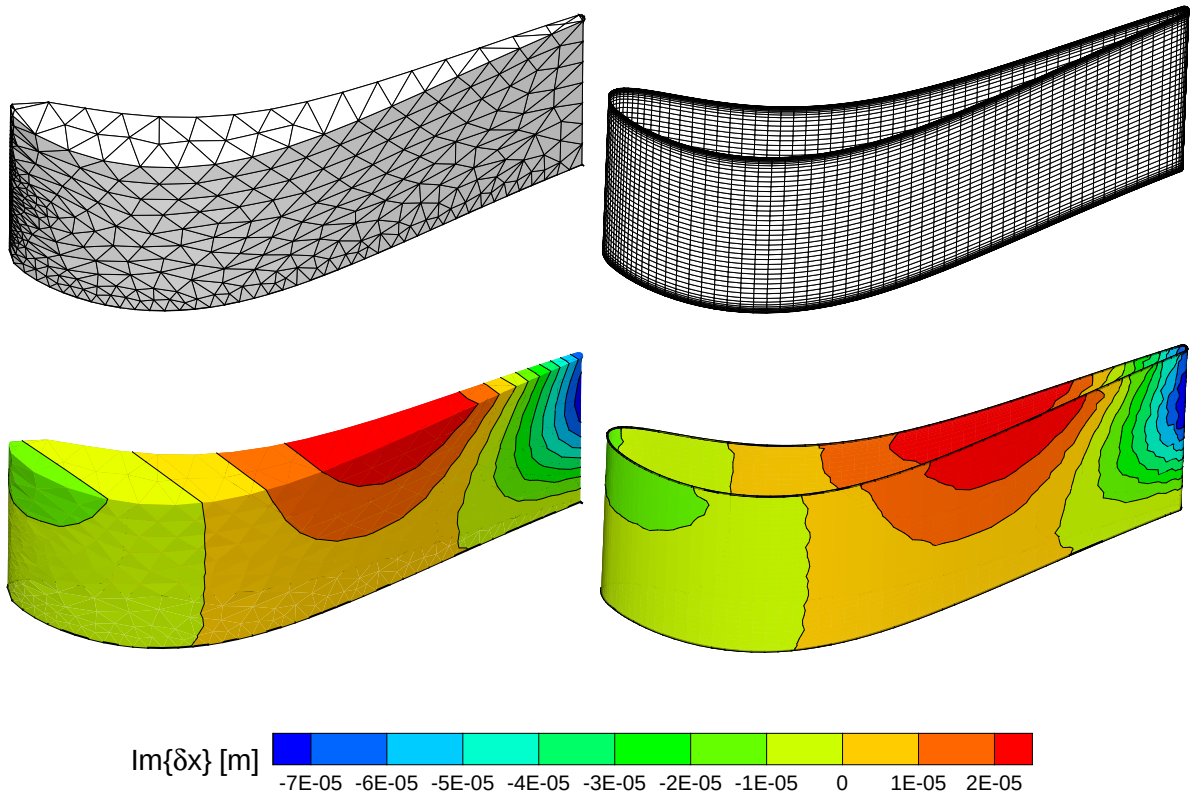

Figure 3: Unstructured CSM grid and data (left) and the surface displacements mapped to the CFD mesh (right).

length. As seen in figure 3 the mapping results in inaccuracies where the CFD solid wall boundaries exceeds the length of the CSM blade model. This setup is often used for first investigations of the aeroelastic stability of a design in iterative optimization. In spite of this geometry inconsitency the results are of sufficient quality.

Figure 4 shows the original and deformed CFD mesh on a circumferential slice at radial tip position of the CSM model blade. The vectors shown on the right are the solution of the deformation module of PREP.

5.2 LOW PRESSURE TURBINE VANE CLUSTER

The aeroelastic verification of welded turbine blades are an important field in turbomachinery design. The stiff coupling of the blades in the cluster results in different eigenmodes compared to single shrouded blades. Thus the CSM calculations have to be performed with the complete cluster. To investigate the stability of a blade cluster in an aeroelastic simulation these mode shapes should be mapped on a similar setup of blades in the CFD domain, see figure 5. In this application the topology independence of the presented approach is the key for the industrial applicability.There is no need to define

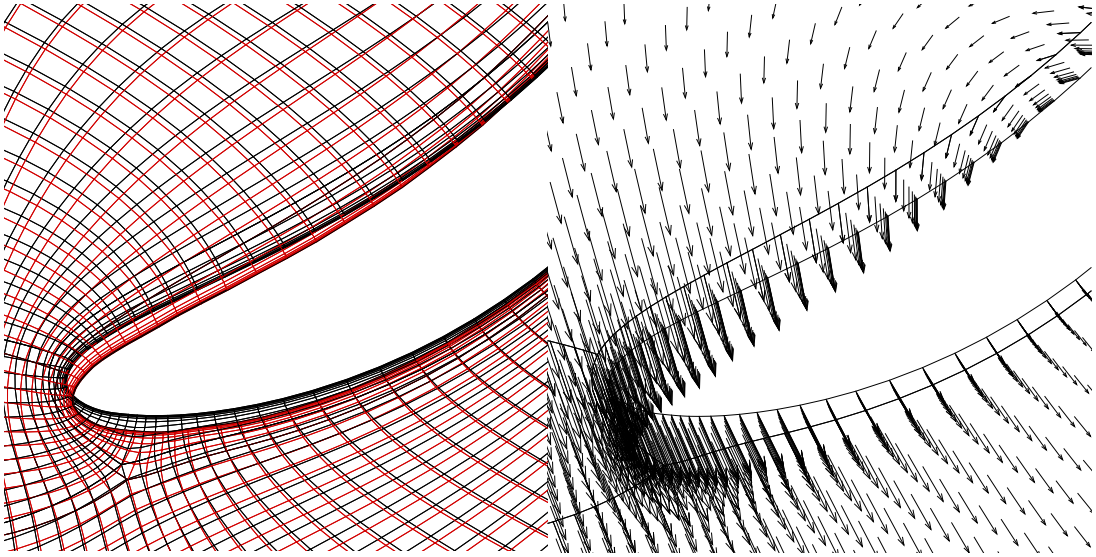

Figure 4: Original CFD mesh (black) and real part of the deformed mesh (displacement scaled by factor 20, red) and the real part of the vectors prescribing this deformation.

leading or trailing edges or the ordering of surfaces and boundaries to lead the mapping. This complex setup can be mapped as precisely and easy as a single blade.

For shrouded blades a mandatory step is to clean the CSM geometry from the shrouds if these are not part of the CFD geometry. The algorithm has a sufficient tolerance against fillets that are part of the structural model but not of the CFD simulation. Major differences in the geometries such as shrouds or roots have to be removed to keep the geometries of CSM and CFD as congruent as possible.

5.3 HIGH PRESSURE FAN

The design of a transonic low bypass fan stage with a very high pressure ratio in a single stage configuration was optimized at the German Aerospace Center's (DLR) Institute of Propulsion Technology[8,9] and tested for its aerodynamic stability at the Institute of Aeroelasticity[10]. Here a brief overview over the aeroelastic process using the timelinearized TRACE solver is given.

First a steady solution for the considered operation point is computed by TRACE. Details of the steady solution are shown in figure 7. Then starting from the mode shape, i.e. the surface displacements computed by CalculiX, and the CFD mesh the process described in the sections above the computation of the deformation is performed by using the aeroelastic pre-processor PREP. The result of the mapping process is shown in figure 6. This step includes the setup of the linear aeroelastic computation, i.e. the interblade phase angle and the frequency is set. With this setup the linear solver is used to compute a perturbation field and the damping coefficient. To compute a complete damping curve

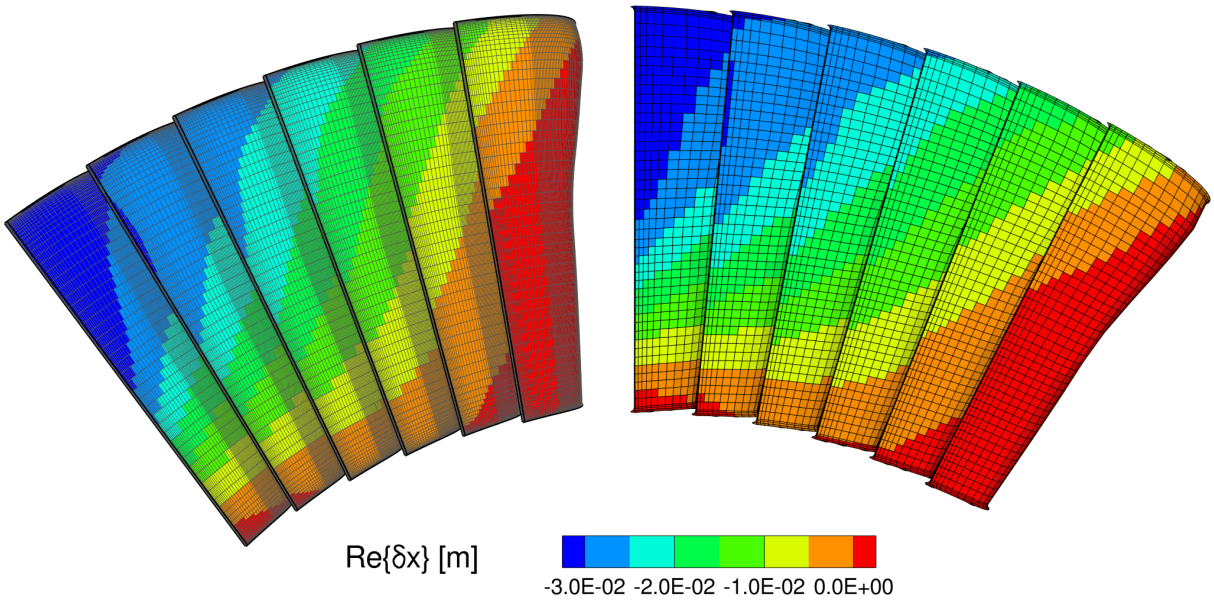

Figure 5: Structured CSM grid and the surface displacements (right) mapped to the CFD mesh (only every second grid line in spanwise direction shown) (left).

the computation of the deformation and the subsequent linear solver step is repeated for each interblade phase angle. The mapping of the surface displacements has not to be performed again if they are independent of the nodal diameter, i.e. independent of the interblade phase angle. The resulting damping curves for the first three mode shapes are given in figure 8.

6 CONCLUSION

A mapping algorithm and an elliptic mesh deformation tool have been developed in order to facilitate the aeroelastic pre-process for arbitrary geometries and topologies. For the three presented applications, a turbine vane stator, a turbine vane cluster and a fan with a high pressure ratio, it was shown that the implemented algorithm works well even under unfavourable conditions like completely unaligned CSM and CFD geometries or meshes with vastly differing sizes of surface elements. Only geometric data, i.e.vertex coordinates and surface elements, have been used to obtain these results and no knowledge about the topology of these cases has been used. This shows that the presented tool is robust with respect to the quality of the input data and therefore highly suitable for use in automatic workflows as required for industrial design processes.

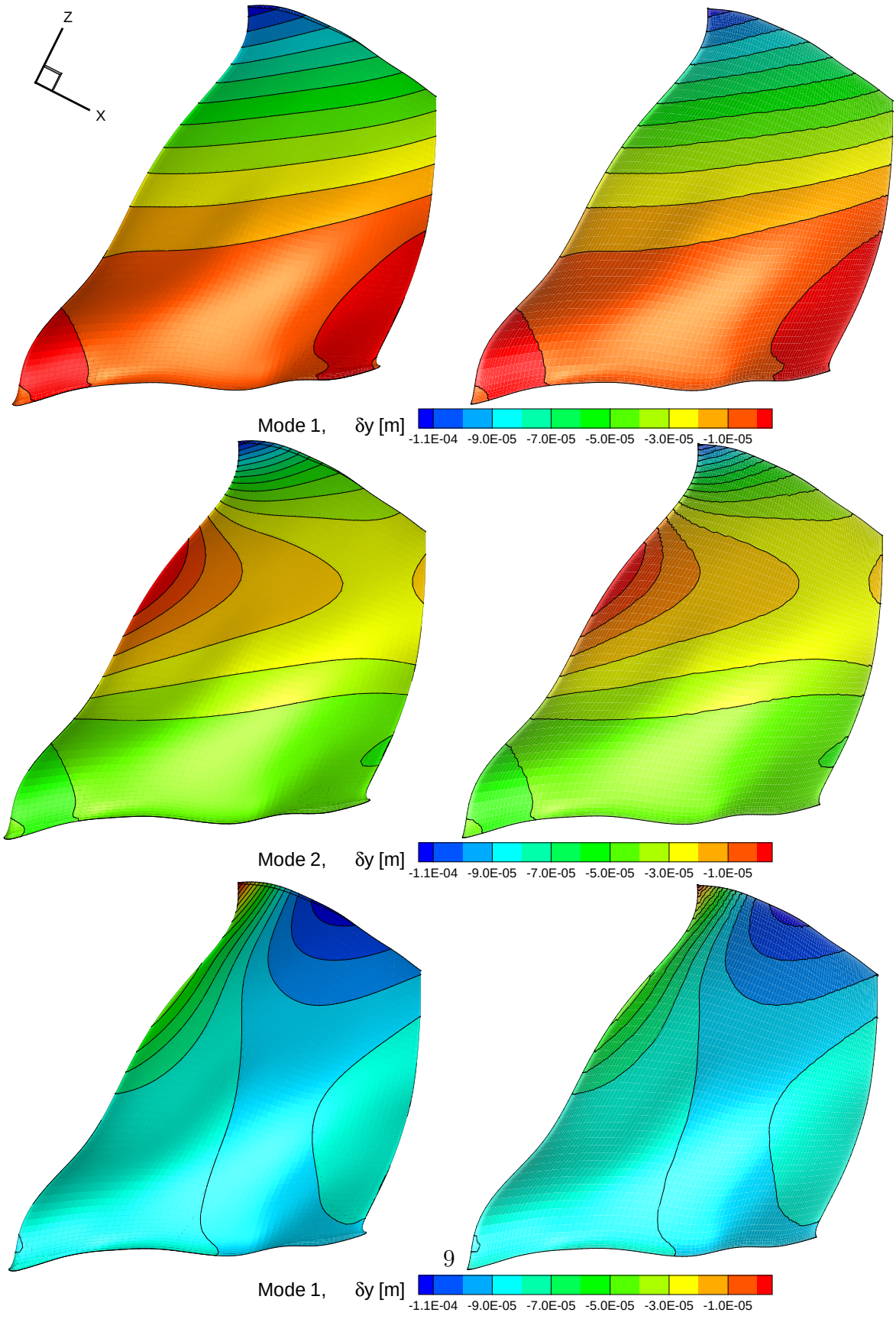

Figure 6: Structured CSM grid and data (left) and the surface displacements mapped to the CFD mesh (right).

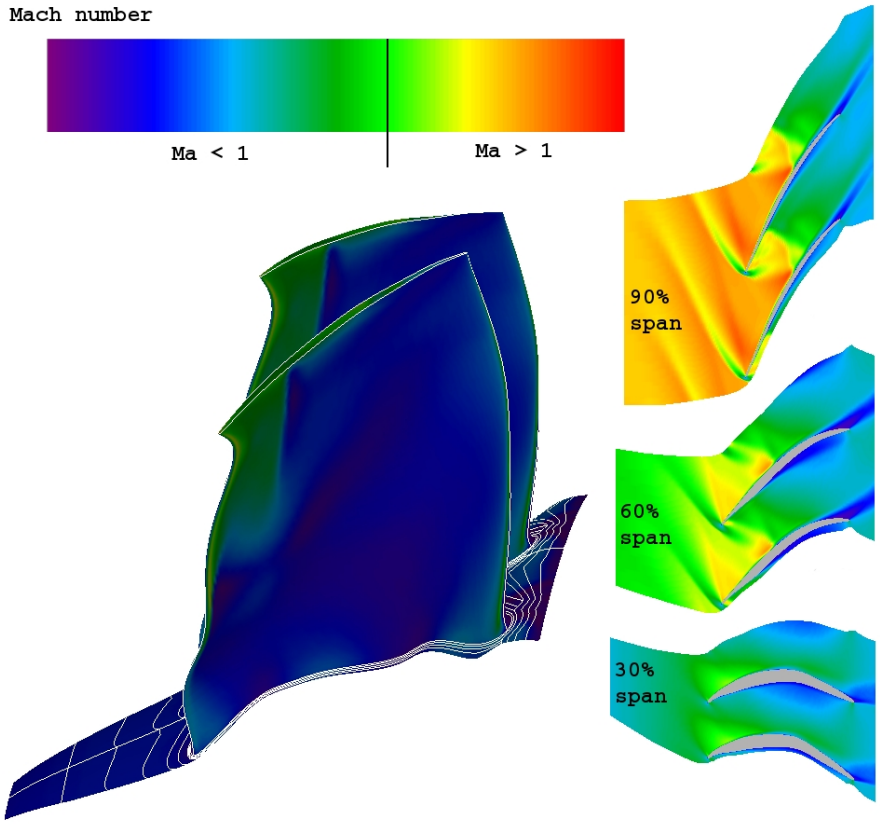

Figure 7: TRACE's steady flow solution as used by the linear solver. (Courtesy of M. May.)

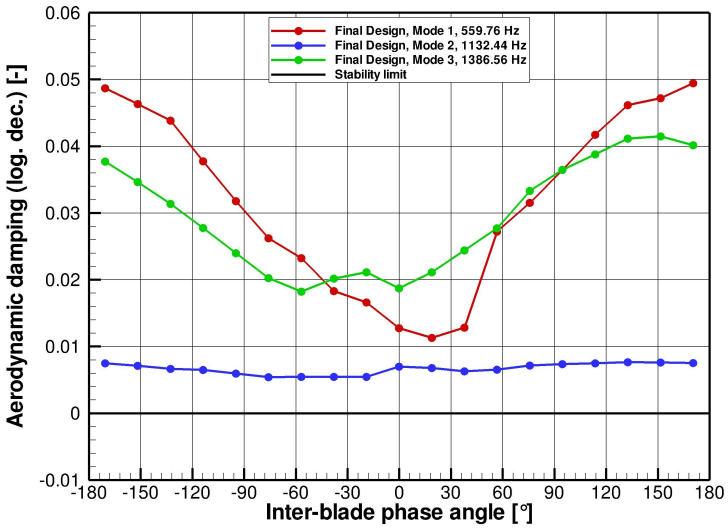

Figure 8: Damping results of TRACE's timelinearized solver for the three modes mapped with PREP. (Courtesy of M. May.)

REFERENCES

[1] Nürnberger, D., Eulitz, F., Schmitt, S., and Zachcial, A., 2001. "Recent Progress in the Numerical Simulation of Unsteady Viscous Multistage Turbomachinery Flow". In 15th International Symposium on Air Breathing Engines, no. ISABE 2001-1081.

[2] Kersken, H.-P., Frey, C., and Voigt, C., 2010. "Time-Linearized and Time-Accurate 3D RANS Methods for Aeroelastic Analysis in Turbomachinery". In ASME Turbo Expo, no. GT2010-22940.

[3] Dhondt, G., 2010. Calculix. http://calculix.de, April.

[4] Fransson, T. H., Jöcker, M., Bölcs, A., and Ott, P., 1999. "Viscous and Inviscid Linear/Nonlinear Calculations Versus Quasi 3D Experimental Data for a new Aeroelastic Turbine Standard Configuration". *Journal of Turbomachinery,* ***121***(1), October, pp. 717–725.

[5] Jöcker, M., 2001. Information for 3D Computations of the STCF 11 Test Cases. Tech. Rep. HPT-11/01, Avdelningen för Kraft- och Värmeteknologi, Kungliga Tekniska Högskolan, Stockholm, SE.

[6] Press, W., Teukolsky, S., Vetterling, W., and Flannery, B., 1992. *Numerical Recipes in C*, 2nd ed. Cambridge University Press, Cambridge, UK.

[7] Yang, Z., and Mavripilis, D. J., 2005. "Unstructured Dynamic Meshes with Higher-order Time Integration Schemes for the Unstready Navier-Stokes Equations". In 43th AIAA Aerospace Sciences Meeting and Exhibit, no. AIAA2005-1222.

[8] Siller, U., Voss, C., and Nicke, E., 2009. "Automated Multidisciplinary Optimization of a Transonic Axial Compressor". In AIAA Aerospace Sciences Meeting, no. AIAA2009-863.

[9] Siller, U., and Aulich, M., 2010. "Multidisciplinary 3d-Optimization of a Fan Stage Performance Map with Consideration of the Static and Dynamic Rotor Mechanics". In ASME Turbo Expo, no. GT2010-22792.

[10] May, M., 2010. "Sensitivity Analysis with Respect to Flutter-free Design of Compressor Blades". In ASME Turbo Expo, no. GT2010-23557.